Proceedings of the 2014 22nd International Conference on Nuclear Engineering
ICONE22
July 7-11, 2014, Prague, Czech Republic

ICONE22-30010

MULTI-GROUP TWO-PHASE FLOW MODEL OF DRIFT DROP PLUME

Vladimir M. Agranat
Applied Computational Fluid Dynamics Analysis
Thornhill, Ontario, Canada

Sergei V. Zhubrin
Applied Computational Fluid Dynamics Analysis
Thornhill, Ontario, Canada

Igor Pioro
University of Ontario Institute of Technology
Oshawa, Ontario, Canada

ABSTRACT

A homogeneous two-phase multi-group model of drift drop plumes emerging from natural draft cooling towers has been developed and validated using the experimental data obtained in the 1977 Chalk Point Dye Tracer Experiment (CPDTE). The conservation equations for mass fractions of water droplets having different sizes are solved in addition to the standard conservation equations for mixture mass, momentum, energy, water vapor mass fraction and turbulent quantities (turbulent kinetic energy and its dissipation rate). Extra terms are provided to the conservation equations for mass fractions of liquid water to account for the drift of water drops due to their gravitational settling. Various formulations for drift velocity and terminal velocity have been tested and compared. The phase change effects (condensation, evaporation, solidification and melting) are assumed to be negligible due to specific conditions of the experiment. The droplet-size distribution available at the cooling tower exit and containing the 25 groups of drops is simplified to 11 groups. Also, the 3-group and 1-group options are considered for comparison. The individual drop deposition fluxes and the total deposition flux are calculated and compared with the experimental data available at the sensors located on the 35° arcs at 500 and 1000 m from the cooling tower centerline. The total deposition flux is calculated as a sum of products of individual group mass concentrations of water drops and corresponding terminal velocities. The model has been incorporated into the commercial general-purpose Computational Fluid Dynamics (CFD) code, PHOENICS. The study has demonstrated a good agreement between the CFD predictions and the experimental data on the water vapor plume rise and the total drift deposition fluxes. In particular, the plume rise predictions agree well with experimental values (the errors are from 4% to 34% at different distances from the tower centerline). The predicted deposition fluxes are in agreement with the experimental values within a factor of 1.5, which is well within the industry acceptable error limits (a factor of 3). The model developed is recommended for analyzing the drift drop plumes under the conditions similar to CPDTE conditions of small Stokes numbers. It is easier to use and not less accurate than the multiphase Eulerian-Lagrangian CFD models used recently by various researchers for modeling CPDTE plume. The model has a potential to supplant or complement the latter in the computational analyses of gravitational phenomena in complex two-phase flows in engineering equipment and its environment.

INTRODUCTION

Over the past three decades, CFD (see Versteeg and Malalasekera (1995) for more details) has been increasingly used as a predictive tool in the analyses of plumes emerging from industrial settings such as cooling towers, etc. It is becoming a validated and user-friendly computational tool in the environmental assessments of dispersion and deposition of pollutants. The standard practice is to use the commercial general-purpose CFD codes such as PHOENICS, ANSYS FLUENT, ANSYS CFX, etc. for such analyses.

In particular, Markatos et al. (1987) used the PHOENICS software for studying the behavior of cooling tower effluent under various environmental and operating conditions. They developed a customized homogeneous two-phase flow model accounting for the water droplet drift via inclusion of additional source terms into the conservation equations for mass concentrations of water vapor and water droplets. The phase change effects were accounted for and the specific formulae

were used for the terminal drop velocity and droplet size growth. The turbulent model used in that paper was the simplest one, i.e. the constant effective turbulent viscosity was specified in the whole computational domain. The authors concluded that the 'results obtained are qualitatively realistic' but 'there are still many uncertainties related to the model, e.g. turbulence and appropriate auxiliary correlations'.

Brown et al. (2003) customized the ANSYS CFX software for CFD prediction of moisture-laden buoyant plumes by applying the homogeneous two-phase mixture model with solving the additional conservation equations for mass fractions of water vapor and liquid water and providing the appropriate source terms accounting for evaporation and condensation. No account was made to calculate the gravitational settling due to small sizes of droplets considered. The k-ε model of turbulence was applied with the buoyancy correction term included (C_3=1).

Meroney (2006) and Lucas et al. (2010) used the FLUENT software for predicting the cooling tower plume rise and drift deposition rates. They applied the Eulerian-Lagrangian multiphase flow option and validated it using the experimental data obtained in the Chalk Point Dye Tracer Experiment (CPDTE) in Maryland, USA during the night of June16-17 in 1977. The standard k-ε model of turbulence was used. These researchers validated their predictive models using the high quality CPDTE data on the sodium/water drift deposition fluxes at the measurement locations, i.e. on the 35° arcs at 500 and 1000 m from the cooling tower centerline. Also, the CFD predictions of plume rise were compared with the experimental data. The CTDTE data on drift deposition flux and plume rise were available from Hanna (1978) and other papers and reports. Meroney (2006) provided a comprehensive description of this validation study.

In this paper, a homogeneous two-phase multi-group model of drift drop plumes emerging from natural draft cooling towers has been developed and implemented into the PHOENICS CFD software (2011 version). The CPDTE data are used to validate the customized model developed and practical recommendations are made on its application for pragmatic prediction of water deposition from a typical natural draft cooling tower. The major model features are described in the next section. The details of CPDTE case study are described in sections 2.0-2.8. It should be noted that PHOENICS was validated for gas release and dispersion applications by Agranat et al. (2007), Tchouvelev et al. (2007) and Houri et al. (2011).

NOMENCLATURE

Put nomenclature here.

1.0 MODEL EQUATIONS

Based on the estimates of Stokes number (see next section) it was concluded that the homogeneous model approach (see definition in Kleinstreuer (2003)) to the CFD modeling of the gas-liquid flow of air with water droplets is applicable to the CPDTE conditions on June 16-17 1997.

The homogeneous CFD model developed consists of the standard conservation equations for mixture mass, momentum, energy, water vapor mass fraction and turbulent quantities (turbulent kinetic energy and its dissipation rate) and the additional conservation equations for mass fractions of water droplets having different sizes. To account for the presence of drops with different sizes a number of additional equations are used. The experimental droplet-size distribution available at the cooling tower exit and containing the 25 groups of drops is simplified to 11 groups, 3 groups and 1 group (see next section). Extra terms are provided to the conservation equations for mass fractions of liquid water to account for the drift of water drops due to their gravitational settling. Various formulations for drift velocity and terminal velocity have been tested and compared (see Annex A). The phase change effects (condensation, evaporation, solidification and melting) are assumed to be negligible due to specific CTDTE conditions on the night of June 16-17, 1977 (93% relative humidity of ambient air). The total drift deposition flux is calculated as a sum of products of individual group mass concentrations of water drops and corresponding terminal velocities.

2.0 MODEL VALIDATION with CPDTE DATA

The CFD model developed was validated using the CPDTE data, that were used by Hanna (1978), Meroney (2006) and Lucas et al. (2010) for validating their models. The CTDTE input data and the experimental values of drift deposition fluxes on the 35° arcs at 500 and 1000 m from the cooling tower centerline were taken from Hanna (1978), Hanna et al. (1982), Meroney (2006) and Lucas et al. (2010).

2.1 Input Data in the CPDTE Case Study

A tall natural-draft cooling tower (124 m tall, 114 m in base diameter and 54.8 m in exit diameter) was used on the night of June 16-17 in 1977 in CPDTRE in order to measure the drift deposition rate at a few downwind locations. The drift is the circulating cooling water drops escaping from the cooling tower. The water with drop sizes from 10 to 1400 micron was carried out of the tower and its deposition was measured at the downwind distances of 500 and 1000 m from the tower centerline. The exit liquid water mass flow rate was about 328 g/s as stated by Lucas et al. (2010) and the exit sodium mass flow rate was 1.86 g/s as mentioned by Hanna (1978) and Meroney (2006). The drop-size distribution at the tower exit is available from Hanna (1978) and Hanna et al. (1982) (see Table 11.1 on page 78). It contains 25 groups of drops with different sizes and percentages of total mass flow rate. The vertical plume velocity was 4.5 m/s and the plume temperature was 308.6 K, implying a virtual temperature of 315.3 K. The use of virtual temperature enables to account for the air humidity. According to Hanna (1978) the virtual temperature is equal to the actual temperature times (1+0.61q), where q is the specific humidity. The ambient temperature was 293 K, the relative humidity was 93% and the ambient virtual temperature was 295.3 K. The wind speed was 8 m/s above the height of 100 m

and almost linear below the height of 100 m with the value of 5 m/s at 50 m height.

The summary of major CPDTE input parameters required for CFD modeling is shown in Table 2.1 and more detailed information on the drop size distribution is provided in Table 2.2.

Table 2.1 Input data summary

Input parameter name	Symbol, unit	Value/Formula
Height of tower above the ground	H, m	124
Diameter of tower base	D_b, m	114
Diameter of tower exit	D, m	54.8
Plume vertical speed at tower exit	W, m/s	4.5
Volumetric flow rate at tower exit	Q, m^3/s	10,608
Wind speed at heights above 100 m	U, m/s	8
Wind speed at heights below 100 m	U, m/s	$U=0.3523z^{0.6781}$
Virtual plume temperature	T_{vp} , °K	315.3
Virtual ambient temperature	T_{va} , °K	295.3
Actual plume temperature	T_p , °K	308.6
Actual ambient temperature	T_a , °K	293
Buoyancy flux	F, m^4/s^3	2102, eq. (3.1)
Gas density at tower exit	ρ_g , kg/m^3	1.11
Laminar kinematic viscosity of mixture	ν, m^2/s	1.55E-5
Molecular weight of air	M, kg/kmol	28.9
Ambient pressure	P, kPa	101
Universal gas constant	R, J/kmol/K	8314
Mass flow rate of water at tower exit	m_w, , kg/s	0.328
Mass flow rate of sodium at tower exit	m_s, , kg/s	1.86E-3
Water mass concentration at tower exit	C_w, kg/m^3	3.09E-5
Sodium mass concentration at tower exit	C_s, kg/m^3	1.75E-7
Mass fraction of water at tower exit	Y_w, kg/kg	2.78E-5
Mass fraction of sodium at tower exit	Y_s, kg/kg	1.57E-7
Number of drop groups in drop-size distribution at tower exit	N	25
Range of drop diameters at tower exit	d_{min} to d_{max} , µm	10 to 1400

The experimental drop-size distribution at the tower exit available from Hanna et al. (1982) (Table 11.1 on page 78) contains 25 groups of drops with sizes from 10 to 1400 µm. It was simplified to the 11-group distribution and then further simplified to 3-group and 1-group distributions as shown in Table 2.2. The drops with sizes from 1200 to 1400 µm were ignored as their mass contribution was only 0.2% of total mass. All three different drop-size distributions (11-, 3- and 1-group options) were used in comparative CFD study.

Table 2.2 Simplified 11-, 3- and 1-group drop-size distributions at cooling tower exit

Number of Groups in Model	Group Number	Drop Diameter Range (µm)	Representative Drop size, µm	Percent of Total Mass
11	1	10-50	30	42.6
11	2	50-90	70	22.3
11	3	90-130	110	10.4
11	4	130-210	170	10.2
11	5	210-270	240	4.0
11	6	270-350	300	2.7
11	7	350-450	400	1.6
11	8	450-600	500	1.6
11	9	600-800	700	1.9
11	10	800-1000	900	1.6
11	11	1000-1200	1100	1.1
3	1	10-130	53	75.3
3	2	130-450	224	18.5
3	3	450-1200	771	6.2
1	1	10-1200	129	100

2.2 Similarity Analysis

The input data listed in Tables 2.1 and 2.2 were used to estimate the terminal velocities and Stokes numbers in the CPDTE case study. Table 2.3 shows the values of terminal velocities, $V_{t,1}$ and $V_{t,2}$, and Stokes numbers, St_1 and St_2, for different drop sizes. $V_{t,1}$ and St_1 were obtained with use of standard Stokes drag law, which is valid in cases of small water drop sizes ($d < 77$ µm) where the drop Reynolds number $Re_d < 1$. In particular, $V_{t,1}=1000/\rho_g*g*d^2/(18\nu)$ and $St_1= V_{t,1}/g*V/L$. $V_{t,2}$ and St_2 were obtained with use of more general empirical correlations for terminal velocity, i.e. Engelmann formulae available in Hanna et al. (1982) (see formulae (11.17)) were used to calculate $V_{t,2}$ and $St_2 = V_{t,2}/g*V/L$. The characteristic flow velocity, V, was equal to the wind speed of 8 m/s and the characteristic length, L, was equal to the exit diameter of 54.8 m. It should be noted that St_1 is equal to the standard Stokes number, St, defined for small drop sizes in the literature (see definition in Kleinstreuer (2003)) and St_2 is its generalization for arbitrary drop sizes. It is seen from Table 2.3 that both Stokes numbers, St_1 and St_2, are smaller than unity for all the drop sizes considered. In particular, $St_2<0.062<<1$ for all drop sizes. Using $St=St_1$ for large drops could lead to significant over-estimations of Stokes number, e.g., at d=1100 µm, St_1 is larger than St_2 by one order of magnitude. Based on the estimates of St_1 and St_2, the application of homogeneous model of two-phase flow described in section 2.0 was considered valid in this validation study as $St_2<<1$ for all drop sizes used in the model (see Table 2.2).

As a result, the differential equations for droplet velocities that are solved in Eulerian-Lagrangian models were reduced at St<<1 to algebraic equations linking the gas and liquid velocities. In homogeneous model, the horizontal velocity components of gas and liquid are equal and the difference between the corresponding vertical velocity components is equal to terminal velocity. The gravitational settling of drops was accounted for algebraically by providing additional source terms in the conservation equations for mass fractions of water drops.

Table 2.3 Estimates of terminal velocities and Stokes numbers for CPDTE case study

Drop Diameter (m)	$V_{t,1}$ (m/s)	$V_{t,2}$ (m/s)	St_1	St_2
7.00E-05	0.1552	0.1480	0.00231	0.00220
1.00E-04	0.3168	0.3017	0.00471	0.00449
5.00E-04	7.919	2.005	0.1178	0.0298
7.00E-04	15.52	2.964	0.2310	0.0441
9.00E-04	25.66	3.575	0.3818	0.0532
1.10E-03	38.33	4.153	0.5704	0.06180

2.3 CFD Model Features

Based on the estimates of Stokes number the homogeneous two-phase multi-group model was applied to model the CPDTE drift drop plume. The 11-, 3- and 1-group drop-size distributions shown in Table 2.2 were used to estimate the effect of number of groups on the model predictions. The two turbulent models were tested: the standard k-ε model and the constant effective turbulent viscosity model (ν_t=0.01 x half width x velocity difference) of Markatos et al. (1987) were applied for comparison. The two drift drop velocity options were compared (see Annex A): the terminal drop velocity and the drift velocity similar to the one used by Markatos et al. (1987). The phase change effects were not accounted for as it was shown by Meroney (2006) and Lucas et al. (2010) that these effects are negligible for the ambient relative humidity of 93% observed during the CPTDE measurements on the night of June 16-17, 1977.

The computational domain (3000 m x 1000 m x 750 m), the cooling tower, the ground, the inlet and the outlet are shown in Figure 2.1. The cooling tower was located on the symmetry plane at a distance of 500 m from the inlet. Its shape was modeled using a cone frustum with a height of 124 m, base diameter of 114 m and an exit diameter of 54.8 m. At the tower exit the constant vertical velocity of 4.5 m/s was specified and the turbulent intensity of 10% was used. The water drift was introduced by a proper drop size distribution from Table 2.2. The power law recommended by Lucas et al. (2010) was used to reproduce the experimental variable inlet velocity below 100 m and the constant velocity of 8 m/s was applied above 100 m (see Table 2.1). The turbulent intensity of 10% was specified at the inlet. The virtual temperatures of 315.3 °K and 295.3 °K were used at the tower exit and the inlet, respectively. The fixed pressure condition was applied at the outlet. Based on the findings of Meroney (2006) and Lucas et al. (2010) the side boundaries and the top boundary were considered as symmetry planes. The no-slip condition and the smooth turbulent wall functions were applied on the ground plane. It should be noted that an increase of effective ground surface roughness height form 0 to 0.02 m did not show any significant change in the modeling results. The probe (red pencil with yellow end) in Figure 2.1 shows a position on the symmetry plane at 500 m from the tower centerline (one of the measurement locations).

Three computational grids were considered to analyse the grid sensitivity: a base grid of 212,500 cells, an intermediate grid of 387,000 cells and a fine grid of 778,050 of cells. The grid size was smaller near the tower and the ground with cell dimensions ranging from 1-3 m (near solid surfaces) to 35-60 m (near domain boundaries). Most of the results were obtained with the base grid as the grid refinement does not result in a significant improvement in the model accuracy.

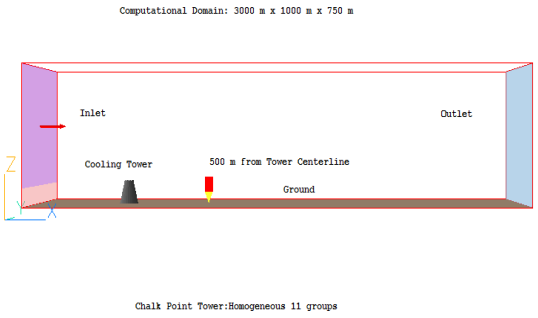

Figure 2.1 CFD domain with cooling tower, ground, inlet and outlet.

2.4 Water Vapor Plume Rise Prediction

The first step in model validation was comparing the predicted water vapor plume rise with the experimental values available at 50, 100 and 200 m from cooling tower centerline. Table 2.4 shows the results of comparison with use of different grid sizes. Also, the comparison was made with the estimates based on the Briggs' formula for buoyancy-dominated bent-over plumes (equation (2.15) in Hanna et al. (1982) and equations (1) and (2) in Hanna (1978)). This standard plume rise formula is provided below for convenience

$$\Delta z=1.6F^{1/3}(\Delta x)^{2/3}/U,\ F=0.25gWD^2(T_{vp}-T_{va})/T_{vp} \qquad (2.1)$$

where Δz is the plume rise above the tower exit, Δx is the downwind distance from tower centerline, U is the wind speed, F is the initial buoyancy flux, g is the acceleration due to gravity, W is the initial plume vertical speed, D is the exit diameter, T_v is the virtual temperature (in °K) and subscripts p and a refer to initial plume and ambient air. Under the CPDTE conditions (Table 2.1), U=8 m/s and F=2102 m^4/s^3. As mentioned by Hanna et al. (1982), the coefficient 1.6 in (2.1) is expected to be accurate within ±40% with variations due to downwash or local terrain effects.

The plume rise was calculated as the vertical position (relative to the tower exit height of 124 m) of the local maximum of predicted relative water vapor mass fraction, C1, at the vertical symmetry plane. It plays an important role in the calculations of maximum ground concentration (Hanna et al (1982)). Table 2.4 shows that the CFD predictions of plume rise agree well with the experimental values available at 50, 100 and 200 m from the tower centerline (Figure 8 in Hanna (1978)) and with the Briggs's formula predictions at 50, 100, 200, 500 and 1000 m. The percentages show agreement with experimental data at distances of 50, 100 and 200 m and with Briggs's formula predictions at distances of 500 and 1000 m where the experimental data were not available. The predictions with k-ε model are more accurate than those with the constant turbulent viscosity model. The increase in computational grid density does not improve the predictions. The CFD predictions are

more conservative than Briggs's formula predictions as they produce smaller values of plume rise and, as a result, larger values of maximum ground concentration are predicted with CFD model.

Table 2.4 Predicted and measured plume rise at various distances from tower centerline

Distance from centerline (m)	Experimental plume rise (m)	Briggs's Formula plume rise (m)	213K grid, k-ε model (Pr_t = 1.0) plume rise (m)	778K grid, k-ε model (Pr_t = 1.0) plume rise (m)
50	30	35 (17%)	32 (7%)	40 (33%)
100	50	55 (10%)	48 (-4%)	48 (-4%)
200	100	87 (-13%)	66 (-34%)	72 (-28%)
500	Not available	160	106 (-34%)	121 (-25%)
1000	Not available	254	198 (-22%)	193 (-24%)

Figure 2.2 shows the 1% and 0.1% iso-surfaces of relative mass fraction of water vapor, C1, obtained with use of standard k-ε turbulent model on a grid of 212,500 cells. The 1% iso-surface does not touch the ground and the 0.1% iso-surface almost strikes it at a distance of about 1480 m from the tower base.

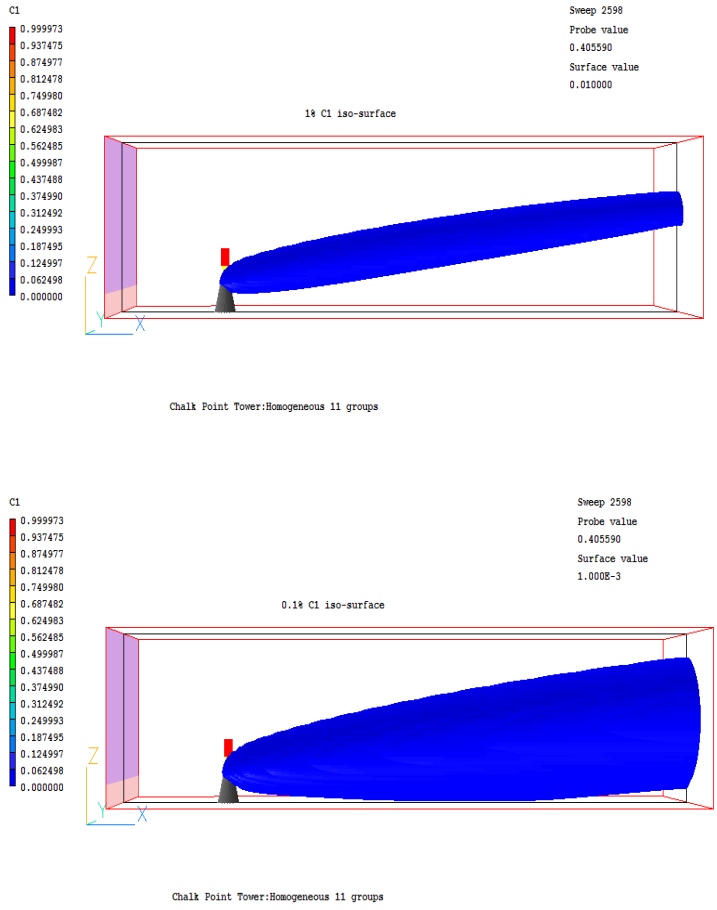

Figure 2.2 Water vapor plume: 1% and 0.1% iso-surfaces of relative mass fraction of water vapor.

The contour of ground-level relative mass fraction of water vapor is shown in Figure 2.3. The maximum is predicted at a distance of about 1480 m from the cooling tower base.

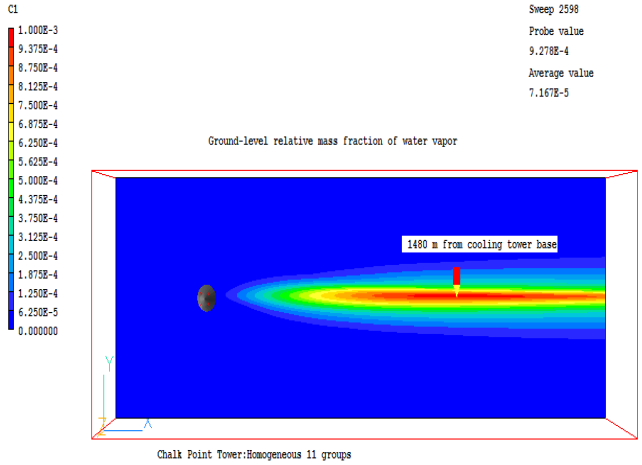

Figure 2.3 Contour of ground-level relative mass fraction of water vapor.

The dependence of ground-level relative mass fraction of water vapor, C1, at symmetry plane on the downwind distance from the tower base is shown in Figure 2.4. The maximum of about 9.8E-4 is predicted at a distance of about 1480 m. It should be mentioned that the maximum is sensitive to the value of turbulent Prandtl number, Pr_t, used in the transport equation for C1: the values of 3.9E-4, 9.8E-4 and 1.9E-3 are predicted at Pr_t values of 1.25, 1.0 and 0.8, respectively.

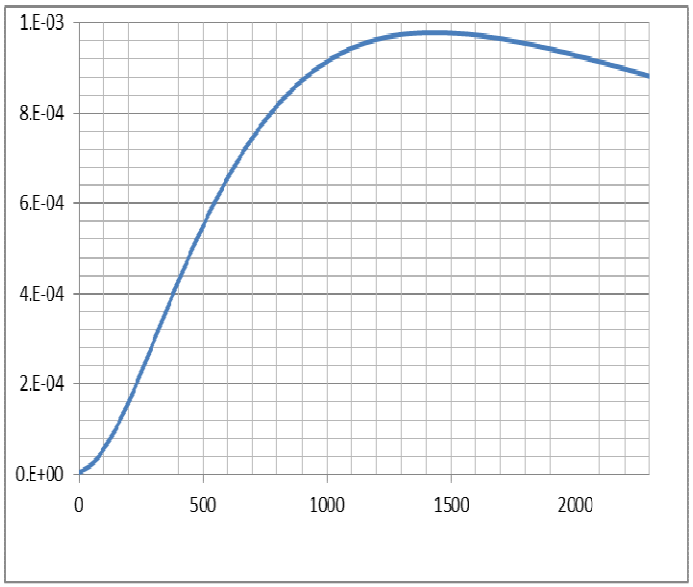

Figure 2.4 Dependence of ground-level relative mass fraction of water vapor, C1, on downwind distance (in m).

2.5 Water/Sodium Deposition Flux Prediction

The CFD model developed was applied to calculate the maximum and average deposition fluxes of water/sodium and these predictions were compared with the experimental values available at the measurement stations located on 35° arcs at 500 and 1000 m from the cooling tower centerline.

The experimental sodium/water deposition fluxes are shown in Table 2.5. It should be noted that Hanna (1978) and Meroney (2006) were comparing their predictions with the experimental average sodium deposition rates and Lucas et al. (2010) were validating their FLUENT model based on the average water deposition rates. Table 2.5 shows both sodium and water deposition fluxes.

Table 2.5 Experimental sodium/water deposition fluxes at 500 and 1000 m from tower centerline

Deposition flux	Unit	Value	Source
Average sodium deposition flux at 500 m on 35° arc	$kg/km^2/mo$	1080	Hanna (1978)
Maximum sodium deposition flux at 500 m on 35° arc	$kg/km^2/mo$	2000	Hanna (1978)
Average sodium deposition flux at 1000 m on 35° arc	$kg/km^2/mo$	330	Hanna (1978)
Maximum sodium deposition flux at 1000 m on 35° arc	$kg/km^2/mo$	667	Hanna (1978)
Average sodium deposition flux at 500 m on 35° arc	$kg/m^2/s$	4.17E-10	1080*3.86E-13
Maximum sodium deposition flux at 500 m on 35° arc	$kg/m^2/s$	7.72E-10	2000*3.86E-13
Average sodium deposition flux at 1000 m on 35° arc	$kg/m^2/s$	1.27E-10	330*3.86E-13
Maximum sodium deposition flux at 1000 m on 35° arc	$kg/m^2/s$	2.57E-10	667*3.86E-13
Average water deposition flux at 500 m on 35° arc	$kg/m^2/s$	7.35E-8	$4.17E\text{-}10*(m_w/m_s)$
Maximum water deposition flux at 500 m on 35° arc	$kg/m^2/s$	1.36E-7	$7.72E\text{-}10*(m_w/m_s)$
Average water deposition flux at 1000 m on 35° arc	$kg/m^2/s$	2.24 E-8	$1.27E\text{-}10*(m_w/m_s)$
Maximum water deposition flux at 1000 m on 35° arc	$kg/m^2/s$	4.52E-8	$2.57E\text{-}10*(m_w/m_s)$

In the CFD model, the water deposition fluxes were calculated at a height of 1 m above the ground at downwind distances of 500 and 1000 m. In particular, the maximum deposition fluxes were calculated as the values at the plume symmetry plane and the average deposition fluxes were calculated along the chords corresponding to the 35° arcs (for simplicity). Table 2.6 shows the comparison of CFD predictions with experimental maximum water deposition fluxes at 500 and 1000 m from the tower centerline. The error factors are shown in bold. The best results were obtained in the 3-group case on a coarse grid of 212,500 cells: the error factor is 0.9 at 500 m and 1.27 at 1000 m. These results are better than the best results obtained by Meroney (2006) with use of Eulerian-Lagrangian model on a grid of 165,000 cells (in a domain of 2000 m long, 1000 m wide and 500 m high): his error factors were 0.75 and 0.5 at 500 and 1000 m respectively. The best results in the 11-group case were obtained on a grid of 778,050 cells: the error factor is 0.82 at 500 m and it is 1.51 at 1000 m. These results are comparable to the results reported by Meroney (2006). The 1-group results (with a representative drop diameter of 129 micron) are acceptable at 1000 m (with error factor of 1.22), but these results could not be considered as acceptable at 500 m as the error factor of 0.29 at 500 m is slightly outside of acceptable range (from 1/3 to 3).

Table 2.6 Predicted and measured maximum water deposition fluxes at 500 and 1000 m from tower centerline

Grid Size (Number of Cells)	Location (m)	CFD flux (N=1) ($kg/s/m^2$)	CFD flux (N=3) ($kg/s/m^2$)	CFD flux (N=11) ($kg/s/m^2$)	Experimental maximum flux ($kg/s/m^2$)
212,500	500	4.13E-8 (**0.30**)	1.22E-7 (**0.90**)	1.37E-7 (**1.01**)	1.36E-7
212,500	1000	5.65E-8 (**1.25**)	5.72E-8 (**1.27**)	7.71E-8 (**1.71**)	4.52E-8
778,050	500	3.97E-8 (**0.29**)	7.96E-8 (**0.59**)	1.12E-7 (**0.82**)	1.36E-7
778,050	1000	5.51E-8 (**1.22**)	5.1E-8 (**1.13**)	6.81E-8 (**1.51**)	4.52E-8

Table 2.7 shows the comparison of experimental water deposition fluxes averaged along the 35 arcs with the CFD values averaged along the corresponding chords (for simplicity) and obtained on a grid of 212,500 cells. The error factors are shown in bold. The agreement is acceptable for 3-group predictions (with error factors of 0.58 and 1.03) and for 11-group predictions (with error factors of 0.65 and 1.35). The error factors of 0.22 and 1.07 were obtained with the 1-group model at distances of 500 and 1000 m. This model is slightly insufficient for accurate predictions (with factors from 1/3 to 3).

Table 2.7 Predicted and measured average water deposition fluxes at 500 and 1000 m from tower centerline

Location (m)	CFD flux (N=1) ($kg/s/m^2$)	CFD flux (N=3) ($kg/s/m^2$)	CFD flux (N=11) ($kg/s/m^2$)	Experimental average flux ($kg/s/m^2$)
500	1.60E-8 (**0.22**)	4.24E-8 (**0.58**)	4.78E-8 (**0.65**)	7.35E-8
1000	2.40E-8 (**1.07**)	2.31E-8 (**1.03**)	3.03E-8 (**1.35**)	2.24E-8

Figure 2.5 shows the contour of total ground-level water deposition mass flux predicted with 11-group drop size distribution using k-ε model on a base grid of 212,500 cells. A value of 1.37E-7 $kg/s/m^2$ is shown by the probe (red pencil with

yellow end) on the symmetry plane at a downwind distance of 500 m from the tower centerline. This value agrees well with the experimental maximum water deposition flux value of 1.36E-7 kg/s/m^2 measured at this location (see Table 2.5).

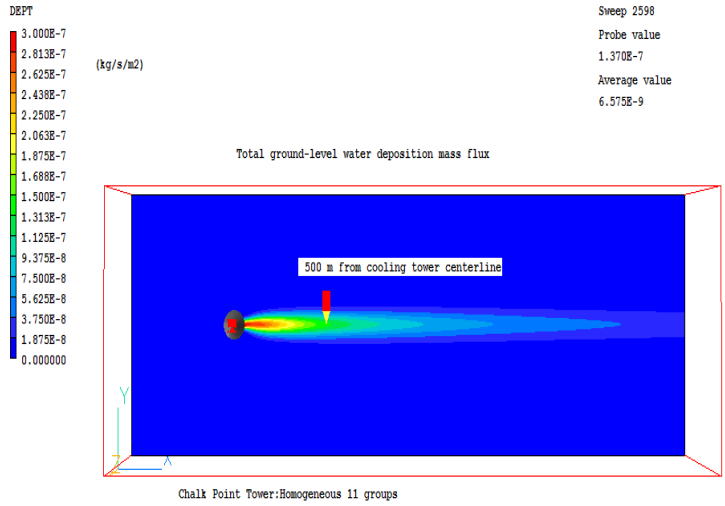

Figure 2.5 Contour of total ground-level water deposition mass flux.

Figure 2.6 shows the 1% iso-surfaces of relative mass fractions of 110, 300, and 900-µm drops (11-group model). It is seen that the 1% iso-surface for 100--µm drops (top picture) is close to the corresponding iso-surface of relative mass fraction of water vapor shown in Figure 2.2. This could be explained by the insignificant gravitational settling of these small drops within computational domain of 3000 m long. The effect of gravitational settling becomes significant for larger drops with sizes of 300 and 900 µm (second and third pictures in Figure 2.6).

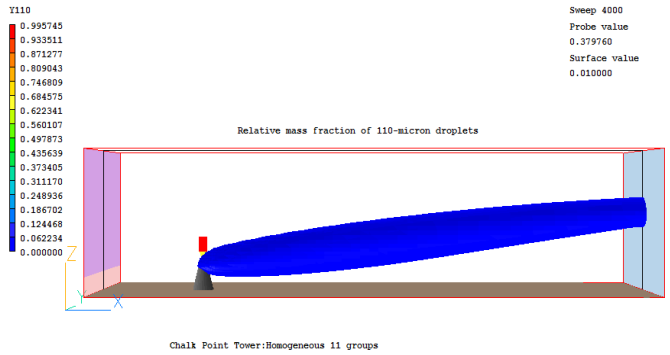

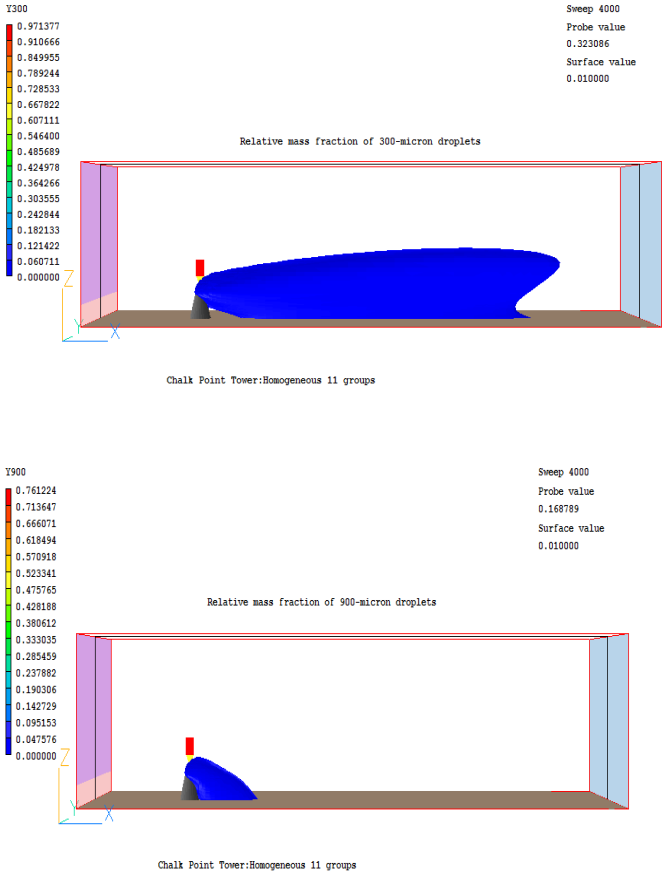

Figure 2.6 1% iso-surfaces of relative mass fractions of 110-, 300-, and 900-micron drops (11-group distribution).

2.6 Effect of Number of Groups on Model Predictions

In order to analyze the effect of number of drop groups on the accuracy of CFD predictions, the maximum water depositions fluxes were calculated with 1-group, 3-group and 11-group distributions on a base grid of 212,500 cells using k-ε model. The predictions are compared in Figure 2.7. It shows that the predictions with 3 groups and 11 groups are close at all the distances from the tower centerline. However, the 1-group predictions close to the 3-group and 11-group predictions only at the distances larger than about 700 m. This is an indication of insufficient accuracy of 1-group model. The 3-group run was also made with using V_d (instead of V_t) in the source terms of conservation equations in order to estimate the effect of drift velocity model. This effect is described in the next section below.

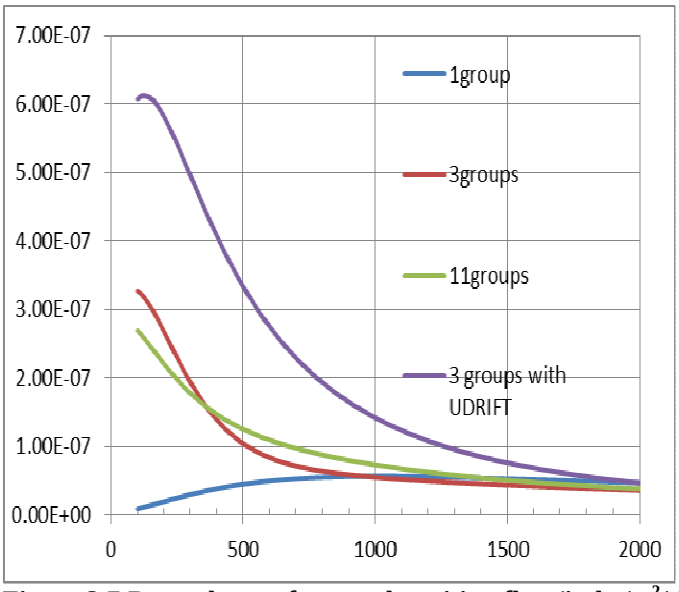

Figure 2.7 Dependence of water deposition flux (in kg/m^2/s) on distance from the tower (in m) predicted with different options of multi-group model (11-group, 3-group and 1-group options).

2.7 Effect of Drift Velocity Model on Model Predictions

Comparison of water deposition fluxes predicted with using the two different formulations of drift velocities (terminal velocity, V_t, and drift velocity, V_d) in the source terms of the conservation equations for relative mass fractions of drops was made in the 3-group case with use of k-ε model on a base grid of 212,500 cells. The values of water deposition fluxes predicted with use of V_d were 3.75E-7 kg/s/m^2 and 1.56E-7 kg/s/m^2 at 500 and 1000 m respectively. These values are about 3 times the values of 1.22E-7 kg/s/m^2 and 5.65E-8 kg/s/m^2 predicted with use of V_t. Figure 2.7 illustrates this difference. The comparison of two modeling options suggests that the use of V_t is preferred with respect to use of V_d.

It should be noted that, in the 1-group case, the use of V_d (instead of V_t) in the source terms results in the values of 4.03E-8 kg/s/m^2 and 5.49E-8 kg/s/m^2 at 500 and 1000 m, respectively. These values are close to the values of 4.13E-8 kg/s/m^2 and 5.65E-8 kg/s/m^2 obtained with use of V_t.

2.8 Effect of Turbulence Model on Model Predictions

Comparison of water deposition fluxes predicted with two different turbulent models (k-ε model and constant turbulent viscosity model) was made in order to estimate the potential use of the simplest turbulent models in practical CFD applications. The effective turbulent viscosity model recommended by Markatos et al. (1987) (ν_t=0.01 x half width x velocity difference) was applied with three modeling options (11-, 3- and 1- group options) on a base grid of 212,500 cells. Table 2.8 shows the predicted and measured maximum deposition fluxes. It is seen that the use of constant turbulent viscosity model is sufficient for accurate predictions of maximum depositions fluxes at 500 and 1000 m from the tower centerline, i.e. all the drop-size options (1-, 3- and 11-group options) result in the acceptable error factors shown in bold (in a range from 1/3 to 3).

Table 2.8 Predicted and measured maximum water deposition fluxes at 500 and 1000 m from tower centerline (constant turbulent viscosity model)

Location (m)	CFD flux (N=1) (kg/s/m^2)	CFD flux (N=3) (kg/s/m^2)	CFD flux (N=11) (kg/s/m^2)	Experimental maximum flux (kg/s/m^2)
500	6.65E-8 (**0.49**)	1.15E-7 (**0.85**)	1.34E-7 (**0.99**)	1.36E-7
1000	7.16E-8 (**1.58**)	6.10E-8 (**1.35**)	7.75E-8 (**1.71**)	4.52E-8

3.0 CONCLUSIONS

1. A homogeneous two-phase multi-group model of drift drop plume has been developed and validated using the CPDTE data obtained in Maryland, USA in 1977.
2. The study has demonstrated a good agreement between the CFD predictions and the experimental data on the water vapor plume rise and the liquid water deposition rates. No model tuning was made for validation purposes.
3. In particular, the plume rise predictions agree well with experimental values and with the standard Briggs's formula for plume rise.
4. The predicted deposition fluxes are in agreement with the experimental values within a factor of 1.5, which is well within the industry acceptable error limits (a factor of 3).
5. The model developed is recommended for analyzing the drift drop plumes under the conditions similar to CPDTE conditions of small Stokes numbers. It is easier to use and as accurate as the multiphase Eulerian-Lagrangian CFD models recently used for modeling the CPDTE plume.
6. The model developed has an advantage of being in a form of fully compatible with methods widely used in CFD practice. The algebraic nature of the model relationships makes it easy bringing them into the computational loops of available predictive tools.
7. From practical point of view, the CFD results obtained with using 3- and 11- group models are acceptable for all three computational grids considered. The details of grid comparison study are shown in Tables 2.4 and 2.6. Theoretically speaking, a more comprehensive grid sensitivity study could be useful and it will be conducted in future.

8. The novelty of presented work (in comparison to previous CFD studies by Markatos et al. (1987), Brown et al. (2003), Meroney (2006) and Lucas et al. (2010)) is in developing and validating a new two-phase multi-group CFD model of water droplet transport and deposition. The new model is easier to use and not less accurate than the previous models.

ACKNOWLEDGMENTS

The authors would like to acknowledge helpful communications and information provided by Dr. Steven Hanna (Hanna Consultants), Prof. Robert Meroney (Colorado State University) and Jeffrey Weil (Research Applications Laboratory at the National Center for Atmospheric Research).

REFERENCES

1. Agranat, V.M., Tchouvelev, A.V., Cheng, Z., and Zhubrin, S.V. (2007), *CFD Modeling of Gas Release and Dispersion: Prediction of Flammable Gas Clouds*, In "Advanced Combustion and Aerothermal Technologies", Syred, N., and Khalatov, A., editors, Springer, Dordrecht, Netherlands, pp. 179-195.

2. Brown, G.J., and Fletcher, D.F. (2003), *CFD Prediction of Odour Dispersion and Plume Visibility for Alumina Refinery Calciner Stacks*, Proceedings of Third International Conference on CFD in the Minerals and Process Industries, CSIRO, Melbourne, Australia, 10-12 December 2003, pp. 111-120.

3. Clift, R., Grace, J.R., and Weber, M.E. (1978), *Bubbles, Drops and Particles*. Academic Press, New York, USA.

4. Gunn, R., and Kinzer, G.D. (1949), *The Terminal Velocity of Fall for Water Droplets in Stagnant Air*, Journal of Meteorology, 6, 243-248.

5. Hanna, S.R. (1978), *A simple drift deposition model applied to the Chalk Point dye tracer experiment*, Environmental Effects of Cooling Tower Plumes, Symposium on, May 2-4, 1978, U. of Maryland, III-105-III-118.

6. Hanna, S.R., Briggs, G.A., and Hoster, R.P. Jr. (1982), *Cooling Tower Plumes and Drift Deposition*, Chapter 11 of Handbook on Atmospheric Diffusion, U.S. Department of Energy, DOE/TIC-1123 (DE82002045), pp.74-80.

7. Hourri, A., Angers, B., Bénard, P., Tchouvelev, A., and Agranat, V. (2011), *Numerical investigation of the flammable extent of semi-confined hydrogen and methane jets*, International Journal of Hydrogen Energy 36 (3), 2567-2572.

8. Kleinstreuer, C., (2003). *Two-Phase Flow: Theory and Applications*, Taylor & Francis Books, Inc., New York. USA.

9. Lucas, M., Martinez, P.J., Ruiz, J., Sanchez-Kaiser, A., and Viedma, A. (2010), *On the influence of psychrometric ambient conditions on cooling tower drift deposition*, International Journal of Heat and Mass Transfer 53 (4), 594-604.

10. Markatos, N.C., Pericleous, K., and Simitovic, R. (1987), *A Hydrometeorological, Three-Dimensional Model of Thermal Energy Releases into Environmental Media*, International Journal for Numerical Methods in Fluids, 7, 263-276.

11. Meroney, R.N. (2006), *CFD Prediction of Cooling Tower Drift*, Journal of Wind Engineering and Industrial Aerodynamics, 94 (6), 463-490.

12. PHOENICS On-Line Information System: www.cham.co.uk/ChmSupport/polis.php.

13. Radosavljevic, D. (1990), *Numerical Simulation of Direct-Contact Natural-Draught Cooling Tower Performance under the Influence of Cross Wind*, PhD Thesis, Imperial College of Science and Technology, London, UK.

14. Reist, P.C. (1984), *Introduction to Aerosol Science*, MacMillan Publishing Company, New York, New York, USA.

15. Tchouvelev, A.V., Cheng, Z., Agranat, V.M., and Zhubrin, S.V. (2007), *Effectiveness of Small Barriers as Means to Reduce Clearance Distances*, International Journal of Hydrogen Energy, 32 (10-11), 1409-1415.

16. Versteeg, H.K., and Malalasekera, W. (1995), *An inroduction to computational fluid dynamics*, Longman, Harlow, UK.

ANNEX A

PARTICLE/DROPLET VELOCITY CALCULATION AT SMALL STOKES NUMBERS

The equations of motion of individual liquid particle/droplet (of diameter d) are the following:

$$\frac{1}{6}\pi d^3\rho_p\frac{du_{1,p}}{dt}=\frac{1}{8}\rho C_D\pi d^2\,\mathrm{Re}_p\,\nu d^{-1}(u_1-u_{1,p})-\frac{1}{6}\pi d^3\frac{\partial P}{\partial x} \quad (1)$$

$$\frac{1}{6}\pi d^3\rho_p\frac{dv_{1,p}}{dt}=\frac{1}{8}\rho C_D\pi d^2\,\mathrm{Re}_p\,\nu d^{-1}(v_1-v_{1,p})-\frac{1}{6}\pi d^3\frac{\partial P}{\partial y} \quad (2)$$

$$\frac{1}{6}\pi d^3\rho_p\frac{dw_{1,p}}{dt}=\frac{1}{8}\rho C_D\pi d^2\,\mathrm{Re}_p\,\nu d^{-1}(w_1-w_{1,p}) -\frac{1}{6}\pi d^3\rho_p((1-\frac{\rho}{\rho_p})g+\frac{1}{\rho_p}\frac{\partial P}{\partial z}) \quad (3)$$

Neglecting the pressure gradient force, these equations could be represented in the following dimensionless form:

$$Stk_1 f^{-1}\frac{d(U_{1,p})}{d\tau}=(U_1-U_{1,p}) \quad (4)$$

$$Stk_1 f^{-1}\frac{d(V_{1,p})}{d\tau}=(V_1-V_{1,p}) \quad (5)$$

$$Stk_1 f^{-1}\frac{d(W_{1,p})}{d\tau}=(W_1-W_{1,p})-V_{t,p}f^{-1}V^{-1}(1-\frac{\rho}{\rho_p}) \quad (6)$$

In the above equations, t is the time, s; $\tau = t/t_s$ is the dimensionless time; $t_s = L/V$ is the characteristic time of gas flow system, s; L is the characteristic length of gas flow system, m; V is the characteristic velocity of gas flow system, m/s; $Stk_1 = t_p/t_s$ is the classical dimensionless Stokes number; $t_p=\rho_p d^2/(18\rho\nu)$ is the classical particle/droplet relaxation time, s; $U_1=u_1/V$, $V_1=v_1/V$ and $W_1=v_1/V$ are the dimensionless velocity components of gas mixture flow, m/s; $U_{1,p}=u_{1,p}/V$, $V_{1,p}=v_{1,p}/V$ and $W_{1,p}=w_{1,p}/V$ are the dimensionless velocity components of particle/droplet, m/s; $g=9.81$ m/s^2 is the gravitational acceleration; ρ_p is the particle/droplet density, kg/m^3; C_D is the drag coefficient; $f=C_D\mathrm{Re}_p/24$ is the dimensionless ratio of drag coefficient to the Stokes law drag coefficient, $24/\mathrm{Re}_p$; $\mathrm{Re}_p = d\,|\mathbf{u_p}-\mathbf{u}|/\nu$ is the particle Reynolds number; $|\mathbf{u_p}-\mathbf{u}|$ is the magnitude of relative particle/droplet velocity vector with respect to the gas flow velocity, m/s; $V_{t,p}= gt_p$ is the terminal velocity of particle calculated under the assumptions of small Reynolds numbers ($\mathrm{Re}_p<1$).

The factor, f, is calculated based on empirical correlations dependent on the particle Reynolds number, Re_p. One of the commonly used correlations for calculating f is available in Clift et al. (1978):

$$f=\frac{C_D\,\mathrm{Re}_p}{24}=1+0.15\,\mathrm{Re}_p^{\,0.687}+\frac{0.42}{1+4.25*10^4\,\mathrm{Re}_p^{\,-1.16}},\quad \mathrm{Re}_p<3.*10^5 \quad (7)$$

Under the conditions of small Stokes numbers ($Stk_1<<f$), the equations (4)-(6) are reduced to the algebraic equations:

$$u_{1,p}=u_1 \quad (8)$$

$$v_{1,p}=v_1 \quad (9)$$

$$w_{1,p}=w_1-V_{t,p}f^{-1}(1-\frac{\rho}{\rho_p})\cong w_1-V_{t,p}f^{-1} \quad (10)$$

It follows from equations (8)-(10) that $\mathrm{Re}_p = d\,|\mathbf{u_p}-\mathbf{u}|/\nu = (dV_{t,p}/\nu)f^{-1}$. In the Stokes regime ($\mathrm{Re}_p<1$), f=1 and $\mathrm{Re}_p = dV_{t,p}/\nu= dgt_p/\nu=gd^3\rho_p/(18\rho\nu^2)$. In a case of water drops in air (under standard conditions), $\mathrm{Re}_p < 1$ if d < 80 µm. For d < 80 µm, correlation (7) is simplified to f=1. In case of larger drops (d >80 µm), equation (7) needs to be solved by iterations with respect to factor, f, while using $\mathrm{Re}_p = (dV_{t,p}/\nu)f^{-1}$ in (7).

The following correlations were used in most CFD runs to calculate the last term in the vertical velocity component (10):

$$V_{t,p}f^{-1}(1-\frac{\rho}{\rho_p})=\left\{\begin{array}{l}\dfrac{gd^2(\rho_p-\rho)}{18\rho\nu}\\ \dfrac{\nu}{d}10^{\frac{\log_{10}(C_D\,\mathrm{Re}_p{}^2)}{1.35}-1}\end{array}\right\} \quad (11)$$

$$\text{for}\left\{\begin{array}{l}d\le 8\cdot10^{-5}m\\ d>8\cdot10^{-5}m\end{array}\right\},\ C_D\,\mathrm{Re}_p{}^2=\frac{4}{3}\frac{gd^3(\rho_p-\rho)}{\rho\nu^2}$$

The first correlation in (11), which is applicable for d < 80 µm, is the Stokes law correlation and the second one, which is valid for d > 80 µm, is an approximation of empirical data presented in Figure 4.3 in Reist (1984).

Also, in a few CFD sensitivity runs, an approach similar to that used by Markatos et al. (1987) was tested. In particular, the term, $V_{t,p}f^{-1}$, in the third equation (10) was replaced by the 'drift velocity', $V_{D,}$ defined by the equation:

$$V_D=\left\|0.0,V_{t,p}f^{-1}-\left\|0.0,w_1\right\|\right\| \quad (12)$$

where symbol $\|\ \|$ stands for the largest of the quantities contained within it.